Photoionization Loss of Mercury's Sodium Exosphere: seasonal observations by MESSENGER and the THEMIS telescope

Jamie M. Jasinski[1,*], Timothy A. Cassidy[2], Jim M. Raines[3], Anna Milillo[4], Leonardo H. Regoli[5], Ryan Dewey[3], James A. Slavin[3], Valeria Mangano[4] and Neil Murphy[1].

1. NASA Jet Propulsion Laboratory, California Institute of Technology, Pasadena, CA, USA.

2. Laboratory of Atmospheric and Space Sciences, University of Colorado Boulder, CO, USA.

3. Dept. of Climate and Space Sciences and Engineering, University of Michigan, MI, USA.

4. INAF/IAPS, Italy.

5. Applied Physics Laboratory, John Hopkins University, MD, USA.

* Corresponding author: Jamie Jasinski (jasinski@jpl.nasa.gov)

Key Points: (140 characters)

- Photoionization can be a significant loss process to the sodium exosphere with peak loss estimates of 4×10^{24} atoms s^{-1}.

- The photoionization loss process of Mercury's sodium exosphere varies throughout the planet's orbit around the Sun.

- More sodium is lost due to photoionization on the inbound leg (true anomaly angle of 180-360º) of Mercury's orbit than the outbound leg.

Abstract

We present the first investigation and quantification of the photoionization loss process to Mercury's sodium exosphere from spacecraft and ground-based observations. We analyze plasma and neutral sodium measurements from NASA's MESSENGER spacecraft and the THEMIS telescope. We find that the sodium ion (Na^+) content and therefore the significance of photoionization varies with Mercury's orbit around the Sun (i.e. true anomaly angle: TAA). Na^+ production is affected by the neutral sodium solar-radiation acceleration loss process. More Na^+ was measured on the inbound leg of Mercury's orbit at 180-360° TAA because less neutral sodium is lost downtail from radiation acceleration. Calculations using results from observations show that the photoionization loss process removes $\sim 10^{24}$ atoms/s from the sodium exosphere (maxima of 4×10^{24} atoms/s), showing that modeling efforts underestimate this loss process. This is an important result as it shows that photoionization is a significant loss process and larger than loss from radiation acceleration.

Plain Language Summary

Mercury has a thin sodium collision-less atmosphere (i.e. an exosphere). A variety of processes add or subtract sodium particles to and from the exosphere. Photoionization is a loss process, and we investigate it in this paper by analyzing data from NASA's MESSENGER spacecraft and ground-based observations made by the THEMIS telescope. Mercury has an eccentric (non-circular) orbit, which means the planet's distance from the Sun changes throughout its orbit. This, first of all, affects how much sodium is lost due to acceleration of neutral sodium by radiation (i.e. how much sodium is accelerated away from Mercury by radiation from the Sun). This subsequently affects how much sodium is left to be photoionized. Therefore, the amount of sodium lost due to photoionization varies throughout a Mercury-year. We calculate that $\sim 10^{24}$ atoms/s of sodium are lost due to photoionization, and that it is a significant loss process in comparison to acceleration by radiation.

1 Introduction
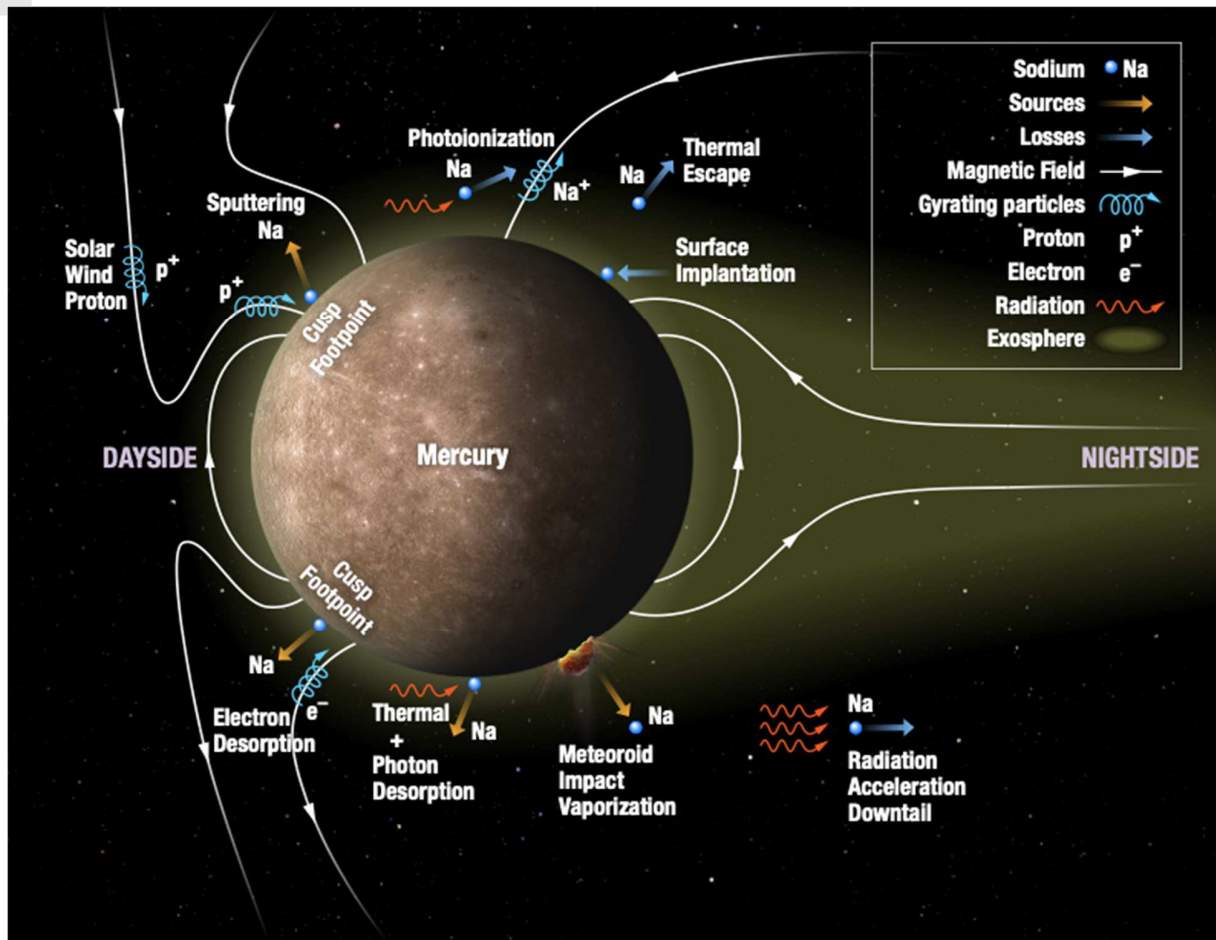
Figure 1. A schematic showing the various exospheric source and loss processes at Mercury.

Mercury has a very tenuous sodium exosphere, where the sodium atoms are more likely to collide with the planetary surface than each other. The neutral sodium exosphere at Mercury is formed from a variety of source and loss processes: Figure 1. Source processes include: photon, thermal, and electron-stimulated desorption, ion sputtering and impact vaporization. Thermal desorption causes atoms to be released from the surface due to heating (Yakshinsky et al., 2000; Leblanc & Johnson, 2003). Photon-stimulated desorption (PSD) and electron-stimulated desorption (ESD) are caused by the transfer of an electron to a higher energy state in a sodium atom after the

bombardment of photons or electrons, respectively, causing desorption of sodium from the surface (McLain et al., 2011; Yakshinskiy and Madey 2000). PSD dominates Mercury's low latitude dayside exosphere production (Leblanc et al., 2006; Cassidy et al., 2015) and is a function of true anomaly angle, TAA (Mura, 2012; Suzuki et al., 2020). Surface release occurs at Mercury due to the coupling between the solar wind and Mercury's magnetosphere. Magnetic reconnection at the dayside injects plasma into the magnetospheric cusps which can precipitate onto the surface of Mercury (Slavin et al., 2014, 2019; Sun et al., 2020) and sputter sodium from the surface. Increased sodium emission has been observed during southward interplanetary magnetic field (IMF) orientations, which are most conducive for reconnection (Mangano et al., 2015; Orsini et al., 2018). Large IMF magnitudes are more likely to produce field-aligned protons which will strike the surface rather than magnetically mirror (Jasinski et al., 2017). Meteroid impact vaporization occurs when a small object strikes the surface of Mercury and causes sodium to be vaporized (Mangano et al., 2007; Jasinski et al., 2020). Micrometeroid impact vaporization is considered another possible major source to the sodium exosphere (Kameda et al., 2009).

Loss processes (Figure 1) remove neutral sodium from the exosphere. Loss processes include: surface implantation, thermal escape, radiation acceleration, and photoionization. Sodium atoms colliding with the surface can be adsorbed (surface implantation). Thermal escape occurs when the thermal energy is sufficiently high (>2.07 eV) to overcome gravitational forces. Radiation acceleration causes sodium to be lost in a cometary-like tail (Potter et al., 2002, 2013; Schleicher et al., 2004; Baumgardner et al., 2008). This is caused by Mercury's orbit which is the most eccentric in the solar system (eccentricity of 0.2 in comparison to Earth's orbital eccentricity of 0.017).

This eccentric orbit, as well as the exospheric emission observed by the UltraViolet and Visible Spectrometer (UVVS) onboard MESSENGER is shown in Figure 2 at various TAAs (0º is at perihelion, 180º at aphelion). The varying radial distance from the Sun results in a varying solar irradiance, which is a factor of 2.3 greater at perihelion then at

aphelion. The eccentricity also means that Mercury has a velocity component directed radially away from the Sun at 0-180º TAA (it is moving away from the Sun and is therefore "outbound") and, has a velocity component directed towards the Sun at 180-360º TAA (it is moving towards the Sun and is "inbound"). This changing radial velocity with respect to the Sun causes the solar spectrum to be Doppler shifted in Mercury's frame of reference. Furthermore, the sodium resonance lines lie in an absorption feature (a Fraunhofer line) of the solar spectrum. This absorption line is shifted to longer and shorter wavelengths on the outbound and inbound portions of its orbit, respectively (Figure 2). Therefore, the solar intensity varies with TAA at the resonance line. Combining this with a varying solar irradiance, results in a varying antisunward acceleration (or g-value) that the neutral sodium experiences with TAA, peaking at 60º and 300º. This changing g-value results in a varying exosphere due to the variation in sodium loss downtail (Potter et al., 2007). Cassidy et al., (2015) found a varying scale height and surface density of neutral sodium at Mercury's dayside which was anti-correlated to the g-value.
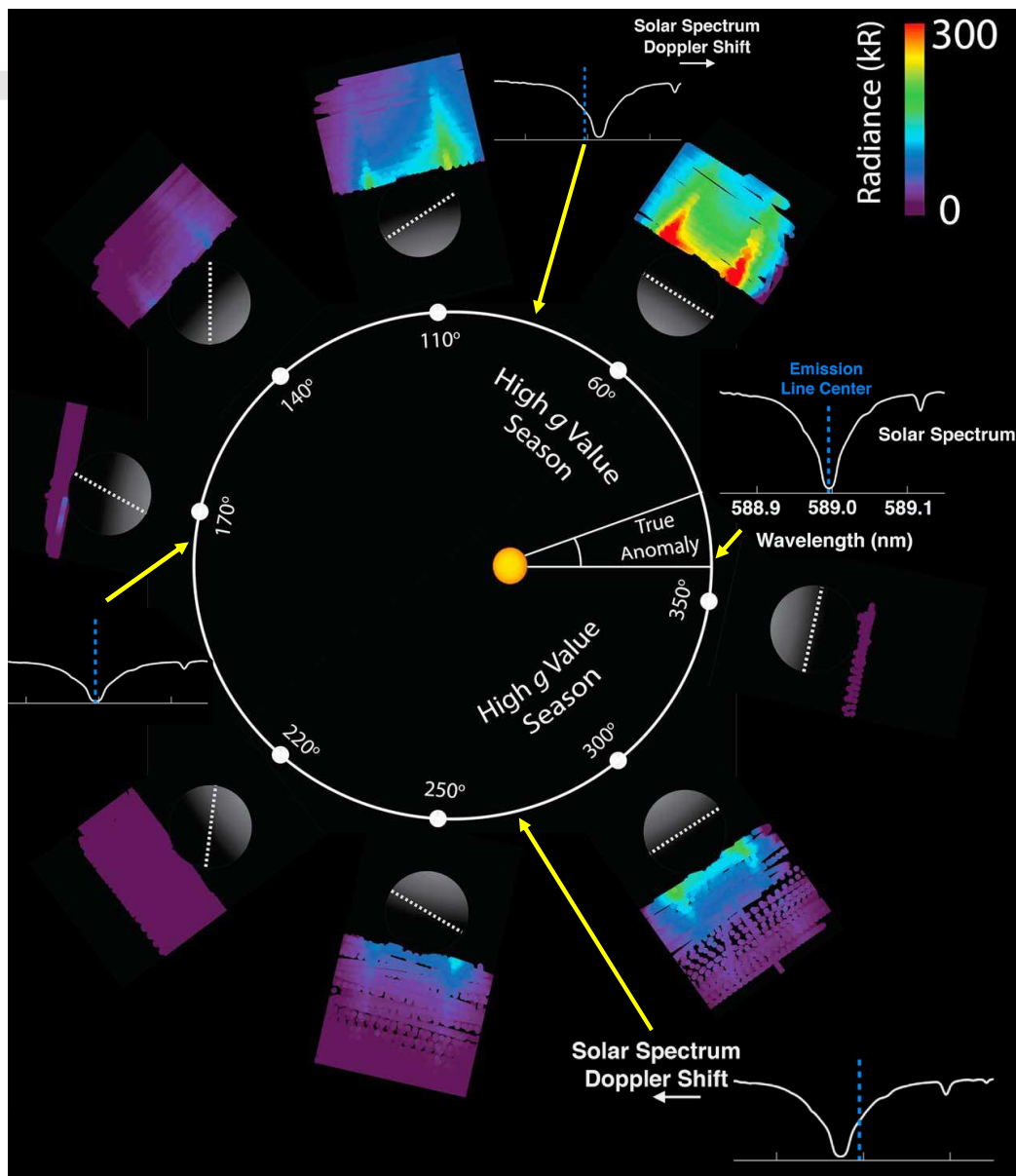
Figure 2. The observed UVVS neutral sodium emission projected onto Mercury's orbital plane, showing the sodium tail which forms during the high g-value portions of Mercury's eccentric orbit. The doppler shift of the solar spectrum at the D2 sodium resonance line (dotted blue line) is also shown at TAAs of 0, 90, 180 and 270º. The white dotted line on Mercury, shows the location of the cold-pole longitudes (longitudes with lower than average temperatures, Peplowski et al, 2014). Adapted from Cassidy et al., (2015, 2016).

Even though there have been many ground and space measurements, the actual quantitative importance of all these sources and losses to the exosphere is ambiguous, largely due to the uncertainties of velocity distributions and sticking coefficients of the atom's interaction with the surface (McClintock et al., 2019). It has been suggested that PSD is the dominant source of the exosphere (McGrath et al., 1987). Impact vaporization has been suggested to contribute 1-20% of the PSD source (Cremonese et al., 2005; Burger et al., 2010; Mouawad et al., 2011). Schmidt et al., (2012) estimated that to populate the lost sodium in the exospheric tail would require 2.7×10^{24} atoms/s from an impact vaporization source or up to 10^{25} atoms/s from PSD. For more information about the exosphere, we refer the reader to recent review chapters (McClintock et al., 2019; Killen et al., 2019).

Photoionization as a loss process to the exosphere has not been previously studied using ion and neutral measurements. Photoionization is the process by which neutral sodium is lost from the exosphere due to the ionization of sodium which is then picked up by the magnetospheric plasma. Using observations from UVVS and the Fast-Imaging Plasma Spectrometer (FIPS) onboard MESSENGER, as well as the ground-based THEMIS solar telescope, we investigate this process. In Section 2 we describe the methods used for analysis. We also present some estimates of the mass loss due to photoionization. In Section 3 we interpret the data and discuss what we have learnt from the results about Mercury's exosphere. In section 4, we summarize our conclusions.

2 Observations and Photoionization-Loss Calculations

In this paper we refer to neutral sodium as "sodium" and sodium ions as "Na$^+$". For this analysis we used data from the following MESSENGER instrumentation: FIPS (Andrews et al., 2007), and UVVS (McClintock et al., 2007). We also use data reported by Milillo et al., (2021) from the THEMIS telescope (López-Ariste et al., 2000). Background information about the instrumentation and the Mercury-Solar-Orbital (MSO) coordinate system can be found in the Online Supporting Material.

2.1 Plasma Measurements and Method

During the MESSENGER mission the northern cusp was observed 2780 times. We use the cusp crossings to analyze the FIPS-measured Na$^+$ count rate dependence with TAA. To account for any orbital or instrument effects that may affect our results, we prescribe certain requirements. Firstly, we only use cusp crossings which measured at least 1 Na$^+$ count. Secondly, since the spacecraft's altitude during cusp crossings varied during the MESSENGER mission, we only use cusp crossings with an average altitude of 0.15-0.25 R_M (a bin width of 244 km). Thirdly, the FIPS instrument had a restricted field-of-view, since it did not have 4π steradian sampling of space. Therefore, we only include cusp crossings when the FIPS boresight vector pointed within 300-30º (i.e. 300-360º, and 0-30º) from the Y_{MSO} direction in the Y-Z_{MSO} plane (0º and 90º being in the Y_{MSO} and Z_{MSO} directions, respectively). This results in observations of ions that have mirrored in the cusp and are largely travelling northwards in the dayside cusp (within a 90º FOV bin). This limits any effects on our results from ion anisotropy in the cusp. These bins were selected so as to retain as much of the data as possible. These requirements result in the analysis of 1452 cusp crossings. We calculate the average Na$^+$ count rate for each cusp crossing (by dividing the total sodium count by the total accumulation time made by FIPS, during a cusp crossing). Figure 3a presents the Na$^+$ count rate binned in 10º TAA bins (where there were at least five cusp crossings). The grey boxes show the interquartile range (IQR), and the whiskers show 1.5xIQR. The red lines show the median Na$^+$ count rate within each TAA bin.

The Na$^+$ count rate in the cusp is used as a proxy for the Na$^+$ content for Mercury's magnetosphere. Estimating a global magnetospheric Na$^+$ content is difficult due to the orbit of MESSENGER (the inclined orbit rotates in local time with TAA) and therefore it is difficult to disentangle the seasonal vs local time variations. If all the Na$^+$ observations from MESSENGER are used, any dependence on TAA will be lost due to local time variations in the magnetosphere. This is seen in Raines et al., (2013; Figure 2c) where dayside and nightside observations are averaged in TAA using different regions (magnetosphere, magnetosheath etc.). This produces a result where magnetospheric local time asymmetries, such as the duskward drift of heavy ions in the magnetotail due to the curvature of the magnetic field, (Delcourt et al., 2003) will be present and any TAA dependency will be lost.

We therefore focus on the northern magnetospheric cusp crossings as it is the only region in Mercury's magnetosphere that is regularly sampled throughout most of Mercury's year, making it a good proxy for the general trend of the Na$^+$ dependency on TAA. We assume the Na$^+$ is generated from photoionization. This is a reasonable assumption: charge-exchange and electron-impact ionization are negligible at Mercury due to the observed low-densities. We also assume that there will be some "magnetospheric processing" of the cusp Na$^+$ (after ionization), which energizes Na$^+$ to the 1-10 keV/q energies observed by FIPS. Even with energization by the magnetosphere the Na$^+$ still originate from photoionization of the sodium exosphere, and our method is justified in understanding sodium in the context of the exosphere.
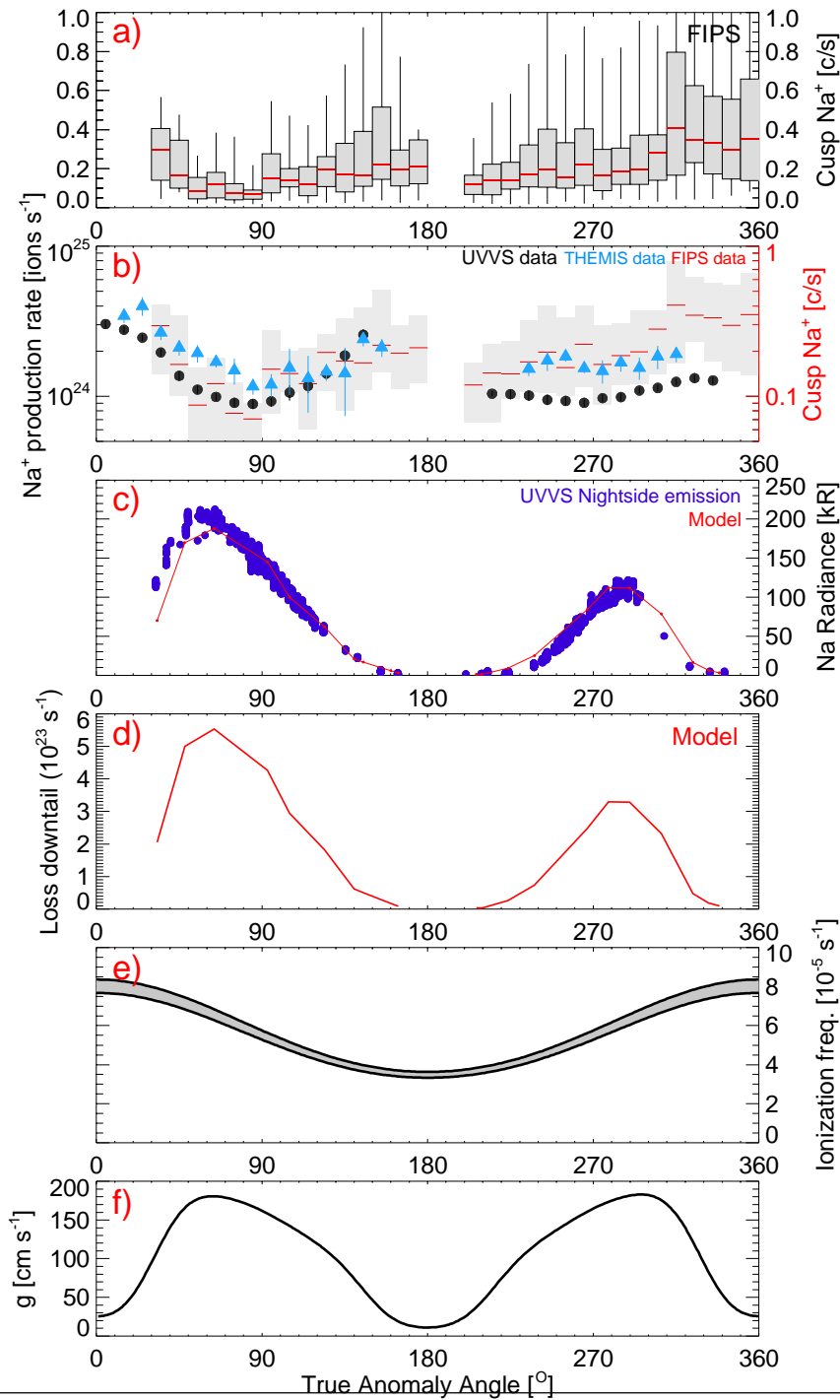
Figure 3. Sodium dependence on TAA. Panel a) FIPS observed Na+ count rate in the cusp binned in 10º TAA bins, (Section 2.1); b) shows the total dayside Na+ production rate (i.e. the amount of ions produced, and therefore neutrals lost from the exosphere) calculated from UVVS measurements (black dots) and the THEMIS telescope (blue triangles). FIPS measurements of Na+ from panel a are also shown again on a log scale for comparison with neutral data. c) UVVS observed nightside emission at midnight local time at 0.25 R_M above Mercury's surface (blue) and a model of nightside emission fit to the data (red); d) modeled sodium loss downtail; e) the ionization frequency of sodium, with the range representative of a quiet and active Sun. f) the solar radiation acceleration of sodium at Mercury.

2.2 Neutral Measurements

2.2.1 Calculation of the ion production rate from photoionization of sodium to Na+

Using UVVS measurements of the sodium density and scale height as they vary in TAA (Cassidy et al., 2015), we calculate an estimate of the mass loss to the exosphere due to photoionization. This is the estimated loss of sodium due to photoionization, consequently leading to the production of Na+. This estimate for the whole dayside exosphere is calculated by taking dayside observations from UVVS data at two-hour local time bins at 0600–1800, using observations at low to mid-latitudes ($\pm 45^0$), and tangent altitudes less than 400km for the whole MESSENGER mission. The data is binned in 10^0 TAA bins (with at least 3 measurements per bin). The measured density and scale height are used to calculate the number of sodium atoms in the local time-latitude volume. The sodium content of the dayside exosphere is then multiplied by the photoionization frequency to calculate the Na+ production rate. We assume the exosphere is optically thin, meaning the photoionization rate is not attenuated with decreasing altitude and remains constant with solar zenith angle and altitude. The optical depth τ, can be calculated using:

$$\tau = \sec \chi \sum_s n_s (z)\sigma_s^a(\lambda)H_s \qquad (1)$$

where χ is the solar zenith angle, z is altitude, n_s is the neutral density, $\sigma_s^a(\lambda)$ is the wavelength-dependent absorption cross section of species s, and H_s is the scale height (Schunk & Nagy, 2000). By using the photoionization cross section (scaled to Mercury's orbital location) for monoatomic sodium from Huebner and Mukherjee (2015) and using an exponential decay approximation for the neutral density and a surface neutral density of 0.9×10^5 cm^{-3} (for TAA=150^0, corresponding to the maximum measured density), the optical depth is $\sim 10^{-5}$. An optical depth equal to unity would mean that the photoionization peak was reached, so a value of 10^{-5} implies that the optically thin approximation is valid. This validates our calculation of the ion production by simply multiplying the ionization frequency by the neutral density.

Figure 3b shows the estimation of the loss due to photoionization (and therefore the Na$^+$ production rate) as black dots. The Na$^+$ production rate estimate from UVVS data does not include the mid-to-high latitude enhancements seen in ground-based datasets. Therefore, we also make the same calculation from ground-based observations using disk-averaged THEMIS-telescope data reduced and analyzed by Mangano et al. (2015) and recently reported by Milillo et al., (2021) which include high latitude regions. Results are shown as blue triangles in Figure 3b. The FIPS-measured Na$^+$ ion count rate are also shown in grey/red on a log-scale (i.e. the data from Figure 3a) for a direct comparison of the three datasets. Details about the uncertainty estimation can be found in the Online Supporting Material.

2.2.2 Nightside emission and downtail loss

Nightside sodium emission observed by UVVS are shown in Figure 3c in blue. UVVS observations at midnight local time and at 0.25 R$_M$ (610 km) altitude were binned in TAA. These measurements were taken when MESSENGER was southward of Mercury and the instrument was facing northward (i.e. "looking upward" towards the limb of the planet). The line-of-sight for these observations include Mercury's umbra (visible in Figure 2). The observed emission comes from sodium in the northern and southern flanks of the tail.

We also used a simple Monte Carlo model (Burger 2021, described by Burger et al., 2014 and used to study sodium by Cassidy et al., 2015) to estimate the sodium loss downtail. The radiance estimated from the model is shown in red (Figure 3c), and the corresponding sodium loss downtail is shown in Figure 3d. We assumed a simplified exosphere source: a 1200 K Maxwell flux distribution centered on the subsolar point and falling off as the cosine of the solar zenith angle (for more information about the model, we refer the reader to the Appendices found in Cassidy et al., 2015). The supply rate was set to match the observed radiance (Figure 3c), which results in a constant supply rate of 6x10^{25} sodium atoms/s. This supply rate assumes that each sodium atom "sticks" when it returns to the surface. In reality atoms are re-ejected and re-desorbed multiple times, an atom can be re-desorbed 20-40 times during its photoionization

lifetime (roughly estimated by dividing the photoionization lifetime by a ballistic lifetime), so the net supply rate is much lower.

Although oversimplified, this model reproduces many features of the UVVS nightside sodium emission data (Figure 3c, model in red; data in blue), most importantly the inbound/outbound asymmetry in tail radiance. This observed emission is of the nightside loss due to radiation acceleration. The loss rate during the outbound leg is about twice that of the inbound (a sodium atom was counted as lost if it traveled more than 15 R_M away from Mercury's center). We found that this outbound/inbound loss ratio is not especially sensitive to the spatial distribution of ejected sodium, but it does change with energy distribution. More energetic sodium produces a smaller ratio while a less energetic source results in a larger ratio. For example, a 600 K source has a ratio of ~5 and a 4000 K source has a ratio of ~1.25. Similar values were described by Schmidt et al. (2012). This model does not reproduce the dawn/dusk asymmetries (Cassidy et al., 2015), latitudinal asymmetries measured by ground-based observers, or the high-energy component seen above the high-altitude dayside (Cassidy et al., 2015) or distant tail (Schmidt et al., 2012).

3. Discussion: what have we learned from the observations?

The results are shown in Figure 3. The Na^+ count rate in the cusp (binned in TAA) is shown in Figure 3a. This is also shown in Figure 3b, alongside the estimated ion production rate at Mercury (i.e. the exospheric loss rate due to photoionization) using neutral measurements from the MESSENGER spacecraft and the Earth-based THEMIS-telescope. Figure 3c shows the nightside sodium emission at altitudes of 0.25 R_M observed by UVVS (blue) and estimated by a simple model (red). Figure 3d shows the estimated sodium loss downtail from this model. For reference, Figure 3e shows the ionization frequency of sodium; where the upper and lower values are for an active and quiet Sun respectively. Figure 3f presents the antisunward g-value experienced by sodium at the exosphere.

Mercury's Na^+ content (Figure 3a) has a large variation for cusp crossings with the same TAA which can be seen by the large IQR (grey boxes). This variation is mostly likely due to magnetospheric effects, where separate isolated orbits may have different magnetospheric activity (i.e. MESSENGER-observed orbit-to-orbit variation). However, the general seasonal TAA-trend of the Na^+ content is affected by the profiles of the g-value (3f) and photoionization frequency (3e). The conditions are more conducive for Na^+ production at 0º (and 360º) TAA when the photoionization frequency is at its highest and when the g-value is at its lowest. If the g-value is lower, less neutral sodium is lost by radiation acceleration, meaning more sodium is available for photoionization. Therefore, at 0 and 360º TAA, increases in the Na^+ count rate are observed. The g-value is also at a minima at 180º TAA. However, the photoionization frequency is also at a minimum, so MESSENGER does not observe as large an increase in Na^+ at 180º as at 0º. When there is a peak in g-value, sodium loss due to acceleration is at its highest, therefore there is less sodium available for photoionization. There is a clear minimum in the Na^+ at 60º when the g-value is at its highest. Similarly, at 300º TAA the g-value is also at a maximum, however the Na^+ does not exhibit a clear depression because there is less sodium lost downtail.

3.1 Different 'effective' g-value between outbound and inbound parts of Mercury's orbit

Even though the g-value at rest with Mercury is equal at TAA's of 60º and 300º, we now explain why more sodium can be lost at 60º than 300º. Figure 2 shows that the solar spectrum is shifted redwards (to longer wavelengths) on outbound TAA's of 0-180º. The solar intensity at the resonance line therefore increases (as it is now on the "blue" side of the Fraunhofer line) and the sodium atom is accelerated. As the sodium atom accelerates away from the Sun, the solar spectrum that the atom observes is shifted further redward and the solar intensity further increases. This feedback loop produces a self-accelerating mechanism where the sodium is further accelerated.

On the inbound portion of Mercury's orbit (180-360º), the solar spectrum is shifted bluewards (towards shorter wavelengths). The solar intensity at the resonance line increases as it now lies on the "red" side of the Fraunhofer line. As the sodium atom is accelerated, the solar spectrum experienced by the atom is redshifted (opposite to the initial bluewards shift) which means the solar intensity at the resonance line is decreased. Consequently, even though the nominal g-value at rest with Mercury can be the same at 60º and 300º TAA, the amount of sodium lost downtail is different. Therefore, the g-value shown in Figure 3f is the g-value for sodium at rest with Mercury (the same at 60º and 30º), whereas the "effective" g-value is the g-value experienced by an atom moving downtail. This mechanism was first proposed by Smyth (1986) and discussed by Smyth and Marconi (1995) and Potter, Killen & Morgan (2007). Even though this mechanism has been discussed in previous publications, it still has consequences on the loss rate from photoionization. As more sodium is lost downtail at 60º than 300º (as seen in Figure 3d), it affects how much neutral sodium is left to be photoionized. Therefore, the measured Na^{+} content by FIPS is higher on the inbound leg (180-360º TAA) in comparison to outbound (0-180º TAA).

3.2 Photoionization: Estimated exospheric loss rates

The estimated dayside loss rate to the exosphere due to photoionization is calculated using surface density and scale height measurements by UVVS (Cassidy et al., 2015), shown in Figure 3b (black dots), and the THEMIS telescope reported by Milillo et al.,

(2021), shown as blue triangles. The estimates generally reproduce the maximum Na$^+$ count rate observed in the FIPS data (grey and red in Figure 3b) at 0º TAA. The estimations also match the trend measured by FIPS very well for 0-180º TAA, with peaks at 0 and 180º and a minima at ~70-80º. During the inbound portion of Mercury's orbit (180-360º), the Na$^+$ production rate from UVVS shows lower values for the Na$^+$ production rate when compared to the FIPS measurements and the estimation from THEMIS. The THEMIS estimation is larger than UVVS because it includes more of the disk due to its high-latitude coverage (UVVS is limited to mid-latitudes). This is also seen for 0-180º where THEMIS consistently estimates higher Na+ production rates. This shows the importance of including high-latitude sodium measurements when investigating Mercury's sodium exosphere. Furthermore, Milillo et al., (2021) find that different regions of Mercury's dayside provide different exospheric sodium contents. Understanding spatial variations is important for future observations and missions, however here we provide a first estimate from data.

The values that such an estimation produces are also important. At its maximum the calculation estimates that exospheric loss values from photoionization alone can be as high as $4x10^{24}$ atoms/s at perihelion (~0º TAA). This is an important result and shows that with such a loss rate, photoionization would result in the total removal of the sodium exosphere within ~4 hours (if other source and loss process were to be "switched off", and the loss rate was kept constant), which is therefore significant. This calculation is made for a dayside sodium exospheric content of ~$4x10^{28}$ atoms, from UVVS estimates of sodium dayside surface density and scale height reported by Cassidy et al., (2015).

Furthermore, only <15% of this Na$^+$ is expected to be recycled back to the surface (Leblanc et al., 2006). Leblanc and Johnson (2003) modeled the exosphere and found an exospheric loss rate due to photoionization of $3.5x10^{23}$ atoms/s, an order of magnitude less than our maximum estimate ($4x10^{24}$ atoms/s), and less than our minimum of $9x10^{23}$ atoms/s (by a factor of 2.5). Similarly, Mura (2012) underestimate Na$^+$ production with an estimated peak value of $8x10^{23}$ s^{-1} (calculated using values from their Table 2). They use larger ionization frequencies which means they underestimate the sodium content of the exosphere. Wurz et al., (2010) mention that 7.45% of the

sodium produced by PSD is lost by photoionization, however they do not specify production rates so we cannot directly compare our results. However, it is clear that models of Mercury's exosphere underestimate the importance of photoionization as a loss process.

When compared to other estimates of mass loss, photoionization is significant depending on the season. In comparison, escape rates due to radiation acceleration have been estimated to be between 5 and 13 x10^{23} atoms/s (Schmidt et al., 2010; Potter & Killen 2008; McClintock et al., 2008). Photoionization-loss values are equal or higher depending on season. The peak escape rate estimated for radiation acceleration occurred at 69º TAA (Schmidt et al., 2010), which is when the loss rate from photoionization is at its lowest. This shows that photoionization is comparable to radiation acceleration as a loss process to the exosphere at 69º TAA and at other TAA's loss due to photoionization is larger.

4 Conclusions

We have completed the first analysis of MESSENGER (FIPS and UVVS) and THEMIS-telescope observations to understand photoionization as a loss mechanism to Mercury's sodium exosphere. Variations in the Na+ that are observed within a single TAA bin are likely due to variation in magnetospheric activity which can vary the Na+ content (i.e. MESSENGER orbit-to-orbit variation). Here we investigated the long-term variations in Na+ depending on Mercury's TAA (i.e. season-to-season variation). We conclude the following:

1. Na+ production varies with Mercury's orbit around the Sun.

2. Na+ production is affected by the g-value. If more neutral sodium is lost downtail due to radiation acceleration then there is less neutral sodium to be photoionized.

3. There is more Na+ production on the inbound leg, which is observed in the MESSENGER plasma measurements. This is due to more neutral sodium which is lost downtail on the outbound leg of Mercury's orbit (0-180º TAA) than on the

inbound (180-360º TAA). This is caused by a self-accelerating mechanism (see Sec. 3.1) on the outbound leg as first proposed by Smyth (1986).

4. Calculations using UVVS and THEMIS-telescope measurements of the sodium exosphere show that exospheric sodium loss rates of ~10^{24} atoms s^{-1} from photoionization (with a peak value of 4×10^{24} atoms s^{-1}) are significant when compared to other loss mechanisms. This value is higher than previous modelled photoionization loss estimates. Photoionization is comparable to radiation acceleration as a loss process to the exosphere at 69º TAA and larger at other TAA's.

5. Despite planetary differences in heliocentric distance, space environment processes, and atmospheric content, the estimated loss of sodium due to photoionization at Mercury is similar to ion loss rates at Venus and Mars (10^{24} - 10^{25} s^{-1}; Futaana et al., 2017; Ramstad et al., 2017).

Although we have focused on the large-scale effects of radiation acceleration affecting photoionization loss, we do expect other effects to contribute to the variation of the sodium exosphere due to spatial or temporal or orbital variations. More accurate and reliable modeling will be the focus of a future paper, including high-latitude enhancements in sodium that can be inferred from other UVVS observation geometries.

References

Andrews, G., Zurbuchen, T. H., Mauk, B. H., Malcom, H., Fisk, L. A., Gloeckler, G., … Raines, J. M. (2007). The energetic particle and plasma spectrometer instrument on the MESSENGER spacecraft. *Space Science Reviews*, **131**, 523. https://doi.org/10.1007/s11214-007-9272-5

Baumgardner, J., Wilson, J. K. and Mendillo, M. (2008). Imaging the sources and full extent of the sodium tail of the planet Mercury. Geophys. Res. Lett., 35, L03201, doi:10.1029/ 2007GL032337.

Burger, M. H., Killen, R. M., Vervack Jr., R. J., Bradley, E. T., McClintock, W. E., Sarantos, M., Benna, M., and Mouawad, N.: Monte Carlo modeling of sodium in Mercury's exosphere during the first two MESSENGER flybys, Icarus, 209, 63–74, https://doi.org/10.1016/j.icarus.2010.05.007, 2010

Burger, M.H., Killen, R.M., McClintock, W.E., Merkel, A.W., Vervack Jr., R.J., Cassidy, T.A., Sarantos, M., 2014. Seasonal variations in Mercury's dayside calcium exosphere. Icarus. http://dx.doi.org/10.1016/j.icarus.2014.04.049.

Burger, M. H. (2021). nexoclom: Neutral Exosphere and Cloud Model (Version 2.3.0). Retrieved from https://github.com/mburger-stsci/nexoclom

Cassidy, T. A., Merkel, A. W., Burger, M. H., Sarantos, M., Killen, R. M., McClintock, W. E., andVervack, R. J. (2015), Mercury's seasonal sodium exosphere: MESSENGER orbital observations, *Icarus*, **248**, 547– 559, doi:10.1016/j.icarus.2014.10.037.

Cassidy, T. A., McClintock, W. E., Killen, R. M., Sarantos, M., Merkel, A. W., Vervack, R. J., and Burger, M. H. (2016), A cold-pole enhancement in Mercury's sodium exosphere, *Geophys. Res. Lett.*, 43, 11,121– 11,128, doi:10.1002/2016GL071071

Cremonese, G., Bruno, M., Mangano, V., Marchi, S., Milillo, A., 2005. Release of neutral sodium

atoms from the surface of Mercury induced by meteoroid impacts. Icarus 177, 122–128.

Delcourt, D. C., Grimald, S., Leblanc, F., Berthelier, J.-J., Millilo, A., Mura, A., … Moore, T. E. (2003). A quantitative model of the planetary Na+ contribution to Mercury's magnetosphere. Annales de Geophysique, 21, 1723– 1736. https://doi.org/doi:10.5194/angeo-21-1723-2003

Futaana, Y., Stenberg Wieser, G., Barabash, S., and Luhmann, J. G. (2017). Solar wind interaction and impact on the Venus atmosphere. Space Science Reviews, 212(3):1453– 1509.

Gamborino, D., Vorburger, A., and Wurz, P.: Mercury's subsolar sodium exosphere: an ab initio calculation to interpret MASCS/UVVS observations from MESSENGER, Ann. Geophys., 37, 455–470, https://doi.org/10.5194/angeo-37-455-2019, (2019).

Huebner, W. F. and Mukherjee, J. (2015). Photoionization and photo- dissociation rates in solar and blackbody radiation fields. Planet. Space Sci., 106, 11–45, doi:10.1016/j.pss.2014.11.022.

Jasinski, J. M., Slavin, J. A., Raines, J. M., & DiBraccio, G. A. (2017). Mercury's solar wind interaction as characterized by magnetospheric plasma mantle observations with MESSENGER. *Journal of Geophysical Research: Space Physics*, 122, 12,153– 12,169. https://doi.org/10.1002/2017JA024594

Jasinski, J.M., Regoli, L.H., Cassidy, T.A. et al. A transient enhancement of Mercury's exosphere at extremely high altitudes inferred from pickup ions. Nat Commun 11, 4350 (2020). https://doi.org/10.1038/s41467-020-18220-2

Kameda, S., Yoshikawa, I., Kagitani, M., and Okano, S. (2009), Interplanetary dust distribution and temporal variability of Mercury's atmospheric Na, Geophys. Res. Lett., 36, L15201, doi:10.1029/2009GL039036.

Killen et al. (2019), Understanding Mercury's Exosphere: Models derived from MESSENGER Observations, Cambridge University Press.

Leblanc, F. and Johnson, R. E. (2003). Mercury's sodium exosphere. Icarus, 164, 261–281, doi:10.1016/S0019-1035(03)00147-7.

Leblanc, F., Delcourt, D., and Johnson, R. E. (2003), Mercury's sodium exosphere: Magnetospheric ion recycling, J. Geophys. Res., 108, 5136, doi:10.1029/2003JE002151, E12

Leblanc, F., Barbieri, C., Cremonese, G., Verani, S., Cosentino, R., Mendillo, M., Sprague, A. and Hunten, D. (2006). Observations of Mercury's exosphere: Spatial distributions and variations of its Na component during August 8, 9 and 10, 2003. Icarus, 185, 395– 402, doi:10.1016/j.icarus.2006.08.006

López-Ariste, A., J. Rayrole, M. Semel First results from THEMIS spectropolarimetric mode A&AS, 142 (2000), pp. 137-148, 10.1051/aas:2000144

Mangano et al., 2007, The contribution of impulsive meteoritic impact vaporization to the Hermean exosphere, Planetary and Space Science, 55, 1541-1556, doi:10.1016/j.pss.2006.10.008

Mangano, V., Massetti, S., Milillo, A., Plainaki, C., Orsini, S., Rispoli, R., and Leblanc, F.: THEMIS Na exosphere observations of Mercury and their correlation with in-situ magnetic field measurements by MESSENGER, Planet. Space Sci., 115, 102–109, https://doi.org/10.1016/j.pss.2015.04.001, 2015.

Marchi, S. A. Morbidelli, G. Cremonese, Flux of meteoroid impacts on Mercury Astron. Astrophys., 431 (I. 3) (2005), pp. 1123-1127

McClintock, W. E., and M. R. Lankton (2007), The Mercury Atmospheric and Surface Composition Spectrometer for the MESSENGER mission, *Space Sci. Rev.*, **131**, 481–521, doi:10.1007/s11214-007-9264-5.

McClintock, W. E., E. T. Bradley, R. J. Vervack, R. M. Killen, A. L. Sprague, N. R. Izenberg, and S. C. Solomon (2008), Mercury's exosphere: Observations during MESSENGER's first Mercury flyby, *Science*, **321**, 92– 94.

McClintock et al., 2019, Observations of Mercury's Exosphere: Composition and Structure, Cambridge University Press.

McGrath, M.A., Johnson, R.E., Lanzerotti, L.J., 1986. Sputtering of sodium on the planet Mercury. Nature 323, 694–696. https://doi.org/10.1038/323694a0

McLain, J. L., Sprague, A. L., Grieves, G. A., Schriver, D., Travinicek, P., and Orlando, T. M. (2011), Electron-stimulated desorption of silicates: A potential source for ions in Mercury's space environment, *J. Geophys. Res.*, 116, E03007, doi:10.1029/2010JE003714

Milillo, A., Mangano, V., Massetti, S., Mura, A., Plainaki, C., Alberti, T., et al. (2021). Exospheric Na distributions along the Mercury orbit with the THEMIS telescope. Icarus, 335, 114179. https://doi.org/10.1016/j.icarus.2020.114179

Mouawad, N., Burger, M. H., Killen, R. M., Potter, A. E., McClintock, W. E., Vervack, R. J., Bradley, E. T., Benna, M., and Naidu, S.: Constraints on Mercury's Na exosphere: Combined MESSENGER and ground-based data, Icarus, 211, 21–36, https://doi.org/10.1016/j.icarus.2010.10.019, 2011.

Mura, A., (2012), Loss rates and time scales for sodium at Mercury, *Planet. Space Sci.*, 63-64, 2– 7, doi:10.1016/j.pss.2011.08.012

Orsini, Stefano; Valeria Mangano, Anna Milillo, Christina Plainaki, Alessandro Mura, Jim M. Raines, Elisabetta De Angelis, Rosanna Rispoli, Francesco Lazzarotto and Alessandro Aronica, Mercury sodium exospheric emission as a proxy for solar perturbations transit, *Scientific Reports*, 10.1038/s41598-018-19163-x, **8**, 1, (2018)

Peplowski, P.N., Evans, L.G., Stockstill-Cahill, K.R., Larence, D.J., Goldsten, J.O., McCoy, T.J., Nittler, L.R., Solomon, S.C., Sprague, A.L., Starr, R.D., Weider, S.Z., 2014. Enhanced sodium abundance in Mercury's north polar region revealed by the MESSENGER

Gamma-Ray Spectrometer. Icarus 228, 86–95.
https://doi.org/10.1016/j.icarus.2013.09.007

Potter, A. E., Killen, R. M. and Morgan, T. H. (2002). The sodium tail of Mercury. Meteorit.
Planet. Sci., 37, 1165–1172, doi:10.1111/ j.1945–5100.2002.tb00886.x.

Potter, A. E., R. M. Killen, and T. H. Morgan (2007), Solar radiation acceleration effects on
Mercury sodium emission, *Icarus*, **186**, 571– 580.

Potter, A. E., and R. M. Killen (2008), Observations of the sodium tail of
Mercury, *Icarus*, **194**, 1– 12.

Potter, A. E., Killen, R. M., Reardon, K. P. and Bida, T. A. (2013). Observation of neutral sodium
above Mercury during the transit of November 8, 2006. Icarus, 226, 172–185,
doi:10.1016/j. icarus.2013.05.029.

Raines, J. M. et al. (2013) Distribution and compositional variations of plasma ions in Mercury's
space environment: the first three Mercury years of MESSENGER observations. J.
Geophys. Res. Space Phys. 118, 1604–1619.

Raines, J. M., Gershman, D. J., Slavin, J. A., Zurbuchen, T. H., Korth, H., Anderson, B. J.,
and Solomon, S. C. (2014), Structure and dynamics of Mercury's magnetospheric cusp:
MESSENGER measurements of protons and planetary ions, *J. Geophys. Res. Space
Physics*, 119, 6587– 6602, doi:10.1002/2014JA020120.

Ramstad, R., S. Barabash, Y. Futaana, H. Nilsson, and M. Holmström. (2017). Global mars-
solar wind coupling and ion escape. Journal of Geophysical Research: Space Physics,
2017JA024306.

Schleicher, H., Wiedemann, G., Wohl, H., Berkefeld, T. and Soltau, D. (2004). Detection of
neutral sodium above Mercury during the transit on 2003 May 7. Astron. Astrophys., 425,
1119–1124, doi:10.1051/0004–6361:20040477.

Schmidt, C. A., Wilson, J. K., Baumgardner, J. and Mendillo, M. (2010). Orbital effects on
Mercury's escaping sodium exosphere. Icarus, 207, 9–16,
doi:10.1016/j.icarus.2009.10.017.

Schmidt, C. A., Baumgardner, J., Mendillo, M. and Wilson, J. K. (2012). Escape rates and
variability constraints for high-energy sodium sources at Mercury. J. Geophys. Res., 117,
A03301, doi:10.1029/2011JA017217.

Schunk, R., & Nagy, A. (2000). Ionospheres: Physics, Plasma Physics, and
Chemistry(Cambridge Atmospheric and Space Science Series). Cambridge: Cambridge
University Press. doi:10.1017/CBO9780511551772

Slavin, J. A. *et al.* MESSENGER observations of Mercury's dayside magnetosphere under
extreme solar wind conditions. *J. Geophys. Res. Space Physics* **119**, 8087–
8116, https://doi.org/10.1002/2014JA020319 (2014).

Slavin, J. A., Middleton, H. R., Raines, J. M., Jia, X., Zhong, J., Sun, W.-J., et al (2019). MESSENGER Observations of Disappearing Dayside Magnetosphere Events at Mercury. *Journal of Geophysical Research: Space Physics*, 124. https://doi.org/10.1029/2019JA026892

Smyth, W.H., 1986. Nature and variability of Mercury's sodium atmosphere. Nature 323, 696–699.

Smyth, W.H., Marconi, M.L., 1995. Theoretical overview and modeling of the sodium and potassium atmospheres of mercury. The Astrophysical Journal 441, 839–864. https://doi.org/10.1086/175407

Sun, W. J., Slavin, J. A., Smith, A. W., Dewey, R. M., Poh, G. K., Jia, X., et al. (2020). Flux transfer event showers at Mercury: Dependence on plasma β and magnetic shear and their contribution to the Dungey cycle. Geophysical Research Letters, 47, e2020GL089784. https://doi.org/10.1029/2020GL089784

Suzuki, Y., Yoshioka, K., Murakami, G., & Yoshikawa, I. (2020). Seasonal variability of Mercury's sodium exosphere deduced from MESSENGER data and numerical simulation. Journal of Geophysical Research: Planets, 125, e2020JE006472. https://doi.org/10.1029/2020JE006472

Yakshinskiy, B. V. and Madey, T. E. (2000). Desorption induced by electronic transitions of Na from SiO_2: Relevance to tenuous planetary atmospheres. Surf. Sci., 451, 160–165.

Solar Spectrum
Doppler Shift

Radiance (kR)
300
0

High *g* Value
Season

True
Anomaly

High *g* Value
Season

110°
60°
140°
170°
220°
250°
300°
350°

Emission
Line Center

Solar Spectrum

588.9 589.0 589.1
Wavelength (nm)

Solar Spectrum
Doppler Shift